Naval Research Laboratory

Washington, DC 20375-5320

NRL/MR/5651--16-9696

Development of an Optically Modulated Scatterer Probe for a Near-Field Measurement System

Mark Patrick

Surface Electronic Warfare Systems Branch
Tactical Electronic Warfare Division

Meredith N. Hutchinson

Photonics Technology Branch
Optical Sciences Division

J. Brad Boos

Electromagnetics Technology Branch
Electronics Science and Technology Division

September 8, 2016

REPORT DOCUMENTATION PAGE

Form Approved
OMB No. 0704-0188

1. REPORT DATE *(DD-MM-YYYY)*	**2. REPORT TYPE**	**3. DATES COVERED** *(From - To)*
08-09-2016	Memorandum	01 November 2014 – 12 March 2015

4. TITLE AND SUBTITLE

Development of an Optically Modulated Scatterer Probe for a Near-Field Measurement System

5a. CONTRACT NUMBER

5b. GRANT NUMBER

5c. PROGRAM ELEMENT NUMBER

6. AUTHOR(S)

Mark Patrick, Meredith N. Hutchinson, and J. Brad Boos

5d. PROJECT NUMBER

5e. TASK NUMBER

5f. WORK UNIT NUMBER
6A21

7. PERFORMING ORGANIZATION NAME(S) AND ADDRESS(ES)

Naval Research Laboratory
4555 Overlook Avenue, SW
Washington, DC 20375-5320

8. PERFORMING ORGANIZATION REPORT NUMBER

NRL/MR/5651--16-9696

9. SPONSORING / MONITORING AGENCY NAME(S) AND ADDRESS(ES)

Office of Naval Research
One Liberty Center
875 North Randolph Street, Suite 1425
Arlington, VA 22203-1995

10. SPONSOR / MONITOR'S ACRONYM(S)

ONR

11. SPONSOR / MONITOR'S REPORT NUMBER(S)

12. DISTRIBUTION / AVAILABILITY STATEMENT

Approved for public release; distribution is unlimited.

13. SUPPLEMENTARY NOTES

14. ABSTRACT

In high-fidelity, near-field measurements, the measurement probe must minimally impact the near-field of the antenna-under-test. To accomplish this, we developed an optically modulated, near-field probe which consists of a rectangular dipole antenna loaded with a photodiode. The modulation scheme separates scattering off of the probe from background reflections. We present the design and performance of an optically modulated scatterer (OMS) probe for use in a near-field measurement system.

15. SUBJECT TERMS
Near-field measurement Antennas
Photodiodes

16. SECURITY CLASSIFICATION OF:			**17. LIMITATION OF ABSTRACT**	**18. NUMBER OF PAGES**	**19a. NAME OF RESPONSIBLE PERSON**
a. REPORT	**b. ABSTRACT**	**c. THIS PAGE**			Meredith N. Hutchinson
Unclassified Unlimited	Unclassified Unlimited	Unclassified Unlimited	Unclassified Unlimited	17	**19b. TELEPHONE NUMBER** *(include area code)* (202) 767-9549

Standard Form 298 (Rev. 8-98)
Prescribed by ANSI Std. Z39.18

CONTENTS

EXECUTIVE SUMMARY

In high-fidelity, near-field measurements, the measurement probe must minimally impact the near-field of the antenna-under-test. To accomplish this, we developed an optically-modulated, near-field probe which consisted of a rectangular dipole antenna loaded with a photodiode. The modulation scheme separates scattering off of the probe from background reflections. We present the design and performance of an optically modulated scatterer (OMS) probe for use in a near-field measurement system. The primary results include:

- Impedance measurements and design details of two photodiodes and the associated optical intensity modulation techniques
- A rectangular dipole antenna design with scattering-amplitude simulations of the photodiode integrated with the antenna
- OMS Probe measurements with discussion on:
    - Near-field pattern measurements of an open-ended waveguide
    - Linearity measurements
    - Future probe design considerations

DEVELOPMENT OF AN OPTICALLY MODULATED SCATTERER PROBE FOR A NEAR-FIELD MEASUREMENT SYSTEM

1. INTRODUCTION

Near-field radiation patterns are useful in diagnosing antenna arrays defects [1], measuring far-field antenna patterns where the far-field is prohibitively far [2], and locating field concentrations in high power microwave applications [3], which could lead to material breakdown. There are two categories of near-field measurements: direct and indirect. In a direct measurement, the field from the antenna-under-test (AUT) is directly measured by a probe whereas, in an indirect measurement, the field is inferred from the scattering off of a probe that is placed in the near-field.

A simple direct measurement method is to use an open-ended waveguide [4] connected to a network analyzer as the receiver. The near-field is measured by spatially scanning either the AUT or the receiver. Reflections off of background objects can be filtered out in the time domain [5]. For array applications, antennas that are smaller than the open-ended waveguide must be used to achieve spacing less than a half wavelength. An array of time-domain sensors has been demonstrated using loop antennas [6]. The metal transmission line from the probe can perturb the very-near-field making the direct measurement approach less favorable than the indirect measurement approach [7].

In an indirect near-field measurement a probe is placed in the near-field and the near-field at the probe is inferred from the scattering off of the probe. These reflections can be measured in either a monostatic or bistatic configuration. In a monostatic configuration, where the transmitting and receiving antenna are both the AUT, the received signal is proportional to the square of the gain of the AUT. Conversely, in a bistatic configuration, where the transmit antenna is the AUT and the receive antenna has a known antenna pattern, the received signal is proportional to the gain of the AUT after normalizing by the antenna pattern of the known receiver. If the scattering strength of the probe is modulated then the reflected signal off of the probe is amplitude modulated and can be isolated from the unmodulated background signals. The probe can either be modulated mechanically [8], electrically [9], or optically [10]. Mechanical modulation is not preferred because it may cause ambiguities in polarization measurements and has a physically limited modulation frequency [8].

When a probe is electrically modulated, the modulation signal is delivered to the probe on bias lines. These bias lines can cause the maximum amplitude response of the probe to shift in frequency and must be accounted for in the probe design [11]. In an optical modulation system, the active element (typically a photodiode) in the probe is modulated by a laser through a fiber optic cable. The photodiode in an optically modulated probe can operate without a bias voltage, which removes the need for bias lines. Additionally, the fiber optic cable that couples the modulation signal onto the probe has no metal which reduces the perturbation on the near-field by the probe compared to an electrically modulated probe with metallic bias lines.

To decrease measurement time, the modulated probes can be assembled into arrays. Both electrically and optically modulated probe arrays have been demonstrated [12, 13]. Each probe could be modulated at a different frequency to measure the field at each probe simultaneously to further reduce measurement time.

Manuscript approved April 22, 2016.

In this paper, we present the design of an optically modulated scatterer (OMS) probe for measuring the near-field pattern of an antenna in a monostatic configuration and demonstrate it with measurements of an open-ended waveguide at 15 GHz. We also provide a path forward to extending this technique to higher frequencies.

2. SYSTEM OVERVIEW

A block diagram of a monostatic, near-field, measurement system with an OMS probe that we built is shown in Fig. 1. An on-off modulated light source delivers an optical signal to the photodiode in the OMS probe which modulates the radar cross-section (RCS) of the OMS probe. The AUT transmits a signal from an RF source into free-space. The return signal consists of a large, unmodulated signal with a small, modulated signal due to the modulation of the RCS of the OMS probe. The unmodulated signal consists of reflections off of objects in the room, including support structures and from the impedance mismatch between the AUT aperture and free-space. The combined modulated and unmodulated signal is down-converted and a narrow-band filter filters out the unmodulated component of the signal. The modulated signal is recorded by a digital lock-in amplifier at the modulation frequency. The amplitude of the measured signal is proportional to the square of the gain of the antenna because the signal is passing through the AUT twice. The OMS probe is raster scanned in a plane in front of the AUT to record the spatial field distribution at a set of discrete points.

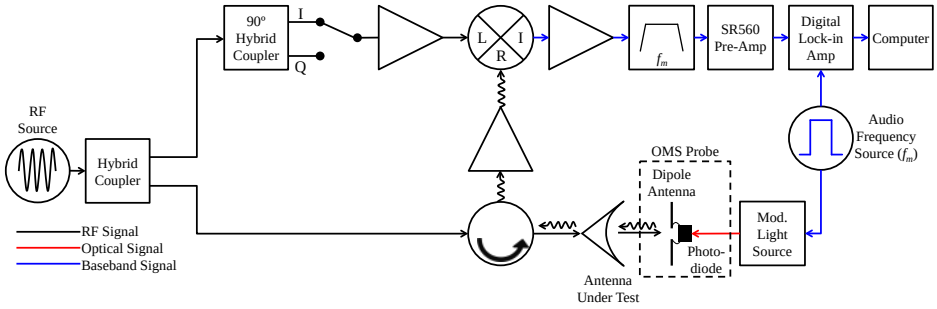

Fig. 1 – A block diagram of the OMS near-field measurement system.

3. PHOTODIODE DESIGN

In a modulated scatterer probe, one design goal is to maximize the difference in the RCS of the probe between the on and off states across the bandwidth of interest which requires a large impedance difference between these states of the active element. Since the purpose of the photodiode incorporated with the probe is to provide large impedance change, investigating different photodiode designs for the desired operation is key to the probe design. We investigated two different styles of photodiodes as the active element in our optically modulated OMS probe. These two styles are a partially depleted absorber (PDA) photodiode and a Modified Uni-Traveling Carrier (MUTC) photodiode, which are typically used in high power analog optical link applications.

3.1 Partially Depleted Absorber (PDA) Photodiode

The first photodiode selected as the active element in our OMS probe was a PDA photodiode. From top to bottom, the layer structure, shown in Fig. 2, is p-doped InP followed by a p-doped InGaAs absorber which gives rise to the PDA design. The intrinsic region is 900 nm of undoped InGaAs followed by the n-doped InP layers. The p-contact is ring style so that the photodiode can be top illuminated. The impedance change between the on and off states of this 32 μm diameter photodiode decreases beyond its bandwidth of 10 GHz. When the photodiode is operated without a bias voltage, strong charge screening effects will induce nonlinearity [14] which can increase the impedance difference between the on and off states – a desirable characteristic for large dynamic range operation of the probe

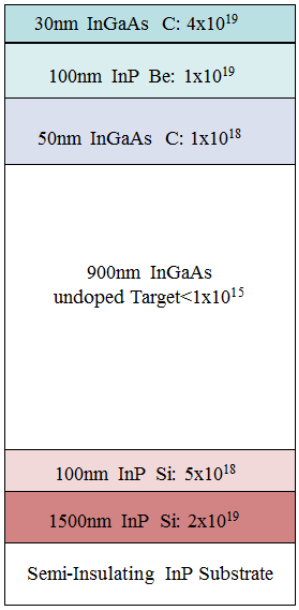

Fig. 2 – Epilayer structure for a PDA photodiode with a 32 μm diameter.

To characterize the photodiode performance, which optimally will have a large change in impedance from 10 GHz to 40 GHz between the on and off states, we calculated the complex impedance, Z, of the unbiased photodiode as a function of frequency and input optical power from $S_{1,1}$ values that we measured with a network analyzer. The $S_{1,1}$ was measured first with no light (off state) and then at different levels of input optical power until no change was observed. The real and imaginary components of the impedance for the PDA photodiode with no light (dark) and at various input optical power levels are shown in Figs. 3 and 4 for 10-20 GHz and 20-40 GHz respectively. The change in impedance decreases as a frequency increases, which indicates that the dynamic range of an OMS probe that is loaded with this PDA photodiode will be limited at higher frequencies. At 10 GHz there was a change in impedance between the dark (off) and maximum optical power (on) states of 40 Ohm in the real component and 80 Ohm in the imaginary component, whereas, at 40 GHz, these changes were 20 and 30 Ohms respectively.

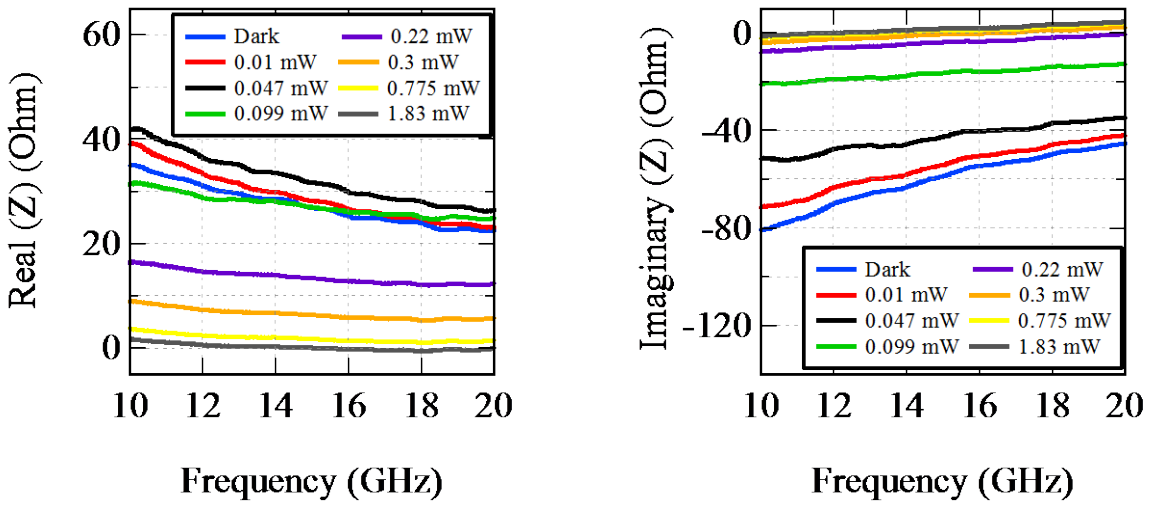

Fig. 3 – PDA photodiode impedance data, real (left) and imaginary (right), as a function of frequency (10 GHz – 20 GHz) and applied optical input power with 0 V bias.

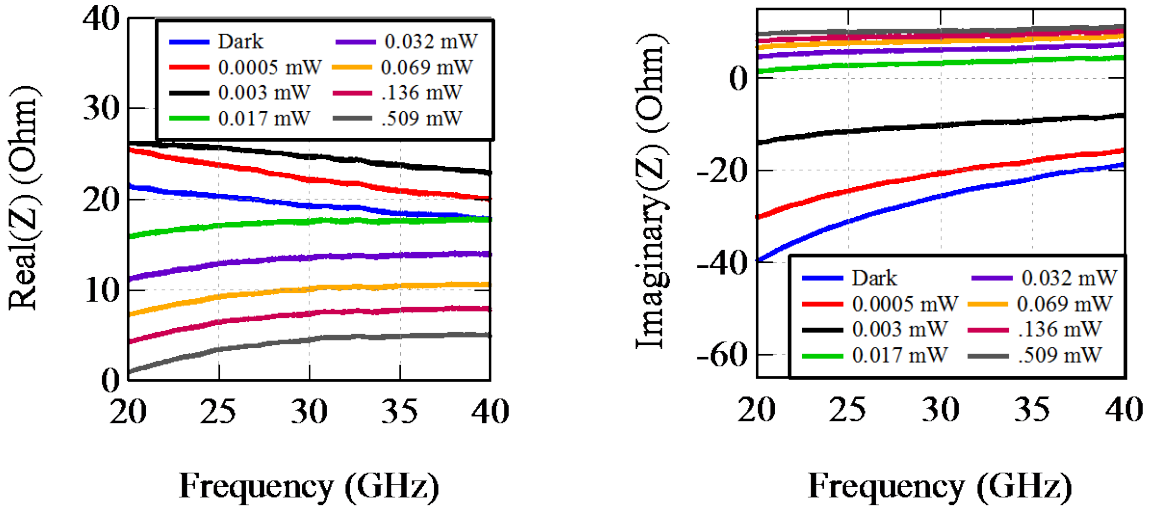

Fig. 4 – PDA photodiode impedance data, real (left) and imaginary (right), as a function of frequency (20 GHz – 40 GHz) and applied optical input power with 0 V bias.

3.2 Modified Uni-Traveling Carrier (MUTC) Photodiode

A second photodiode was selected for use in our OMS probe that had a higher bandwidth to compare against the lower bandwidth PDA photodiode. This photodiode was an InP/InGaAs MUTC photodiode, which are preferred for high power applications [15]. The MUTC layer structure is shown in Fig. 5 (from [15]). From top to bottom, the first two layers are highly p-doped, followed by band smoothing quarternary layers (InGaAsP) to avoid band discontinuities. Next are the InGaAs p-absorber layers where graded doping is employed to induce an electric-field to facilitate transport of electrons into the intrinsic region. There is a small undoped absorbing layer to help with charge balancing which enables higher power operation, where typically space charge can lead to electric field screening. The majority of the intrinsic region is InP, followed by the InP n-region. A small InGaAs layer is included to act as an etch

stop layer for the p-mesa. The photodiode was fabricated and then flip-chip bonded onto an AlN substrate to alleviate thermal effects. The photodiode is 28 μm in diameter. Since the photodiode is designed for high power applications, both its linearity and bandwidth improve at high power. The bandwidth under typical high power (~80 mW) operation is 32 GHz and the bandwidth for low power (≤ 30 mW) operation is 19 GHz.

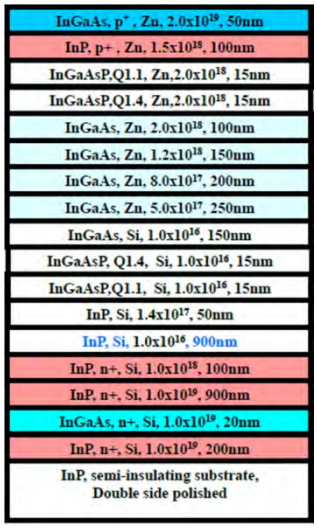

Fig. 5 – Epilayer structure for MUTC photodiode with 28 μm diameter. Reproduced from [15].

In order to characterize the dynamic range of the OMS probe, we first assessed the overall impedance change as a function of the on- and off-state of the photodiode as a function of frequency. We calculated the complex impedance of the MUTC photodiode from measurements of the $S_{1,1}$ of the unbiased MUTC photodiode from 10 to 40 GHz with a network analyzer. The real and imaginary components of the impedance from 10-20 GHz and 20-40 GHz are shown in Figs. 6 and 7 respectively. The real component of impedance changes by about 2 Ohm from 10 to 20 GHz. There change in the real component of impedance modestly increases at 40 GHz – there is an 8 Ohm difference between dark and highest optical power states. This photodiode has a much smaller change in impedance between the on and off states than the PDA photodiode. However, the change in impedance between the off and on states increases as frequency increases. This increase demonstrates that it is more advantageous to operate this photodiode above its operating bandwidth.

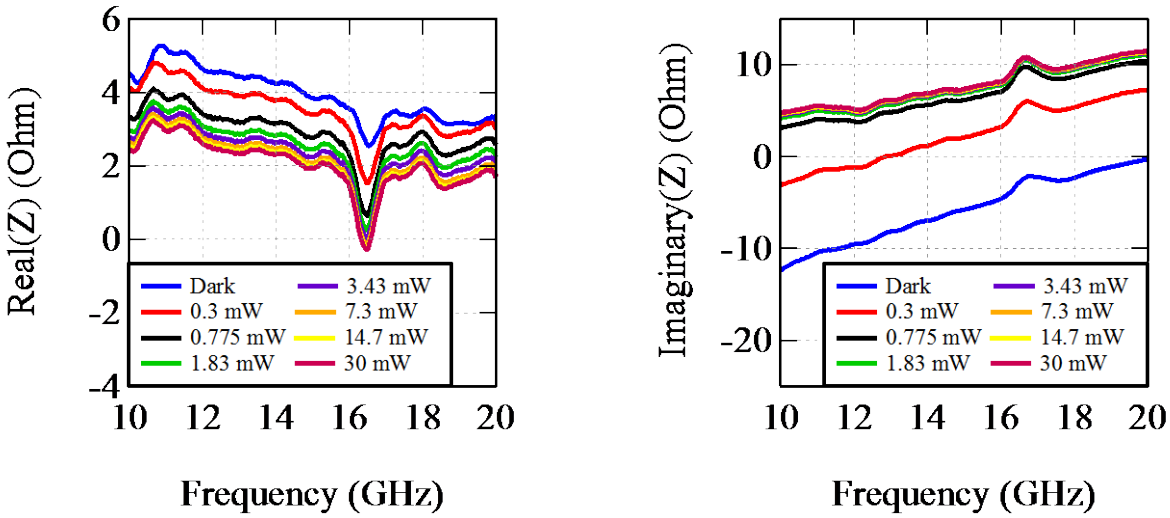

Fig. 6 – MUTC photodiode impedance data, real (left) and imaginary (right), as a function of frequency (10 GHz – 20 GHz) and applied optical input power with 0 V bias.

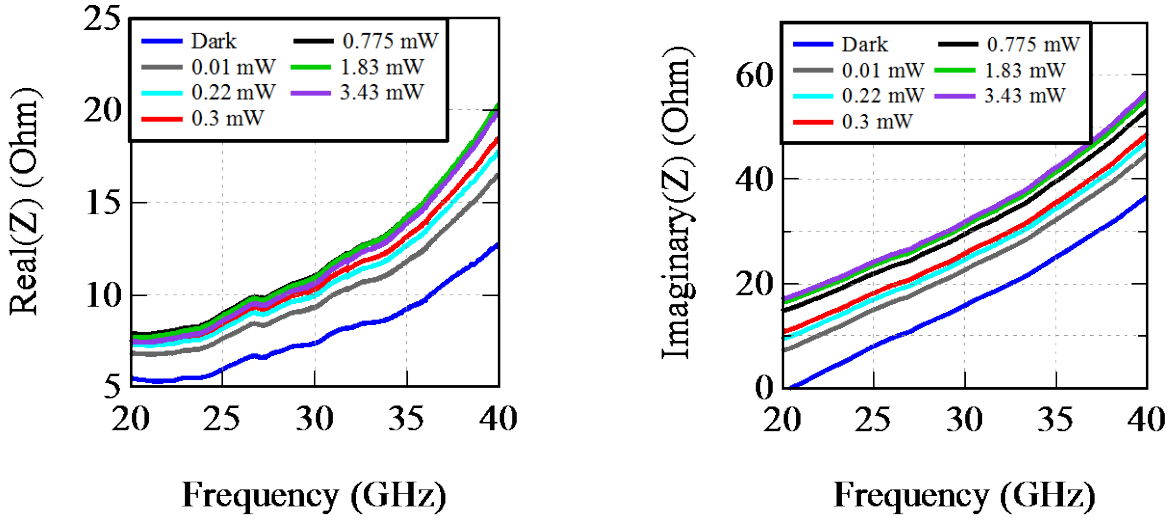

Fig. 7 – MUTC photodiode impedance data, real (left) and imaginary (right), as a function of frequency (20 GHz – 40 GHz) and applied optical input power with 0 V bias.

3.3 Photodiode Modulation

The optically modulated signal is achieved by intensity modulating the output of a continuous-wave (CW) laser. In order to provide a sufficient optical signal to the photodiode, we used a distributed feedback laser (DFB) with 100 mW of optical output power with a wavelength of 1550 nm (Emcore 1782). Since the prototype is an unpackaged photodiode wire-bonded to a dipole antenna the intensity modulated output was coupled to the photodiode with a standard single mode fiber via 3D printed structures which are described in a later section. The modulated optical power incident on the photodiode alternates between the on and off state which results in the largest change in the impedance of the photodiode. For a given maximum optical power, the intensity modulator extinction ratio – the ratio of

power in the on state to the off state – determines the optical power in the off state. For the PDA photodiode with an incident power of ~500 μW, the change in the imaginary component of impedance between the on and off states is 10 Ohms lower for an extinction ratio of 30 dB than it is for an infinite extinction ratio.

Initially, for the intensity modulator, we used a Mach-Zehnder modulator (MZM) that was designed for use in optical links [16], which typically operates below 100% modulation depth. An MZM can be modulated at a higher modulation depth, however the fundamental transfer function is sinusoidal. Increasing the modulation depth and forcing a more square wave output results in distortion in the link which manifests as third order nonlinearity which may negatively affect the probe performance [17, 18]. To achieve the maximum extinction ratio of 30 dB for the MZM, a feedback loop on one of the output ports of the MZM is required to reduce the drift over time of the extinction ratio. The MZM has the advantage of a large bandwidth (20 GHz) which enables fast switching. A switch speed that is larger than the extent in frequency of the phase noise of the RF source (~10 MHz) can improve noise performance.

For a simpler approach, we then used a 1x2 solid-state fiber optic switch (FOS) (Agiltron 1x2 NanoSpeed Switch) to modulate the optical power. The FOS has a maximum repetition rate of 500 kHz and a typical extinction ratio of 25 dB with a maximum of 30 dB. The FOS has a square wave output with a rise/fall time is 300 ns. The extinction ratio of the MZM and FOS are similar but the MZM required the additional complexity of a feedback loop to achieve an equivalent extinction ratio.

4. ANTENNA DESIGN

The antenna in an OMS probe needs to respond at a wide range of angles which makes a dipole antenna an attractive choice [7]. We chose to use a rectangular dipole as the antenna in our OMS probe because it could easily be made using standard printed circuit board (PCB) processing. There are four dimensions in the design of the rectangular dipole antenna: total length, width, gap, and thickness. Figure 8 shows a diagram with the dimensions for the rectangular dipole used as the antenna for our OMS probes. The material used for the antenna was 1 ounce copper (34 μm thick) with a gold finish. The gap between the conductive antenna elements was made wide enough to give the option to mount the PDA photodiode between the conductive antenna elements (the gap was 0.41 mm for a photodiode size of 0.33 mm). The sampling spacing, and therefore the antenna size, must be less than half of a wavelength for near-field measurements – smaller probes increase the spatial resolution of the near-field measurement but have a smaller reflection amplitude [7]. This OMS probe was designed for use in Ku-band (12.4 – 18 GHz). The length of the antenna is 8.03 mm – slightly less than half of a wavelength at 18 GHz. The width of the antenna was then varied to maximize reflection of the on-state for the PDA photodiode at the lower edge of the band (~12.4 GHz) resulting in a probe width of 0.76 mm. This maximum reflection occurred at the frequency where the impedance of the OMS probe was purely real. We constructed two OMS probes, each with a photodiode from the previous sections, and identical antenna dimensions.

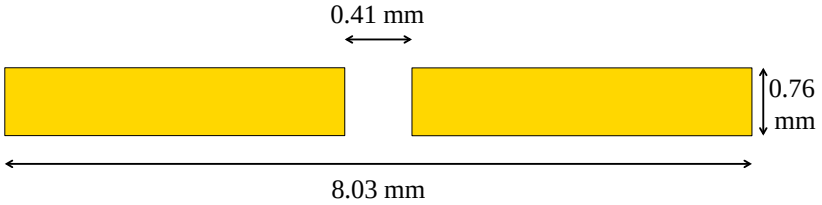

Fig. 8 – Dimensions of the rectangular dipole antenna used in the PDA and MUTC loaded OMS probes.

We simulated the monostatic RCS of each OMS probe, including the antenna element, a photodiode, and the connecting bond wires as a function of frequency in HFSS. The two bond wires that connected the antenna conductive elements to the photodiode were each 25.4 μm thick gold wire with a length of 1.5 mm. The photodiodes were simulated as an impedance sheet between the two bond wires. The non-active elements of the probe were not included in the simulation (the dielectric of the PCB and the material backing the photodiode). The *k*-vector of the incident plane wave was perpendicular to the face of the OMS probe and the polarization was parallel to the long dimension of the antenna.

Figure 9a shows the simulated monostatic RCS for the PDA loaded OMS probe from 10 to 20 GHz. The on-state of this probe has a resonance near the Ku-band lower edge (~12.4 GHz). The off state (dark state) has an amplitude that is lower but a broader frequency resonance at 15 GHz.

The received signal in the near-field system (from Fig. 1) is proportional to the difference of the RCS between the on and off states of the probe. This difference in the RCS of the probe is denoted by the black curve in Fig 9. The frequency response for the difference state of this probe has a narrow peak around 12.4 GHz and a broader peak from 15-18 GHz, which is lower than the 12.4 GHz peak by less than 10 dB. This probe has difference state RCS that is within 10 dB of the maximum value across Ku-band, excluding the 400 MHz null between 13.7 to 14.1 GHz.

Figure 9b shows the results of the same simulation with the MUTC photodiode substituted for the PDA photodiode. The RCS for the on and the off state are higher in amplitude than for the PDA photodiode loaded probe. However, the shift in resonance between the on and off state is 200 MHz in this case as opposed to the 2.6 GHz in the PDA loaded probe case, which is due to the antenna dimensions not being optimized specifically for the impedance of this photodiode. The difference state RCS for the MUTC loaded probe at 12.4, 15, and 18 GHz is lower than the PDA loaded probe by 9, 7, and 15 dB, respectively.

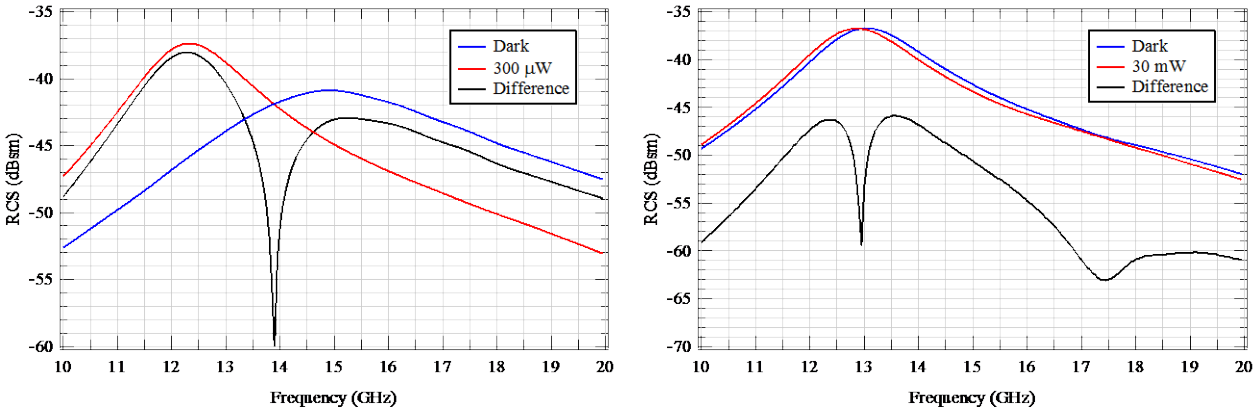

Fig. 9 – Simulated, monostatic RCS for the rectangular dipole antenna, with bondwires, loaded with the measured impedance data from the (a) PDA and (b) MUTC photodiodes for the on and off states and their difference.

5. MOUNTING AND ALIGNMENT

The OMS probe and optical fiber mounting components were designed to have a minimal impact on the near-field of the AUT. To accomplish this, all of the mounting components near the AUT were 3D printed using dielectric material (Vera-White-Plus). The only metal of the OMS probe was from the metal backing of the photodiode and the rectangular dipole antenna.

Figure 10a shows the mounted OMS probe with the coupled fiber in front of a Ka-band standard gain horn and Fig. 10b shows a Solidworks model of the probe and optical fiber mounting components. The probe is glued into the square opening of the probe mount; the optical fiber rests in a V-shaped groove in the fiber mount. The base of the fiber mount fits into a standard optical post holder that is mounted onto a 3-axis micrometer for alignment with the active area on the OMS probe. The alignment of the fiber is performed by moving each axis of the 3-axis micrometer until the received signal is maximized. The power of the laser is then increased further until the received signal no longer increases. Both the probe and fiber structures are mounted on the same 2D positioner stages. The stages are built to have 300 mm of horizontal travel and 50.8 mm of vertical travel. The stage is 101.6 mm below the probe to minimize the impact on the near-field of the AUT.

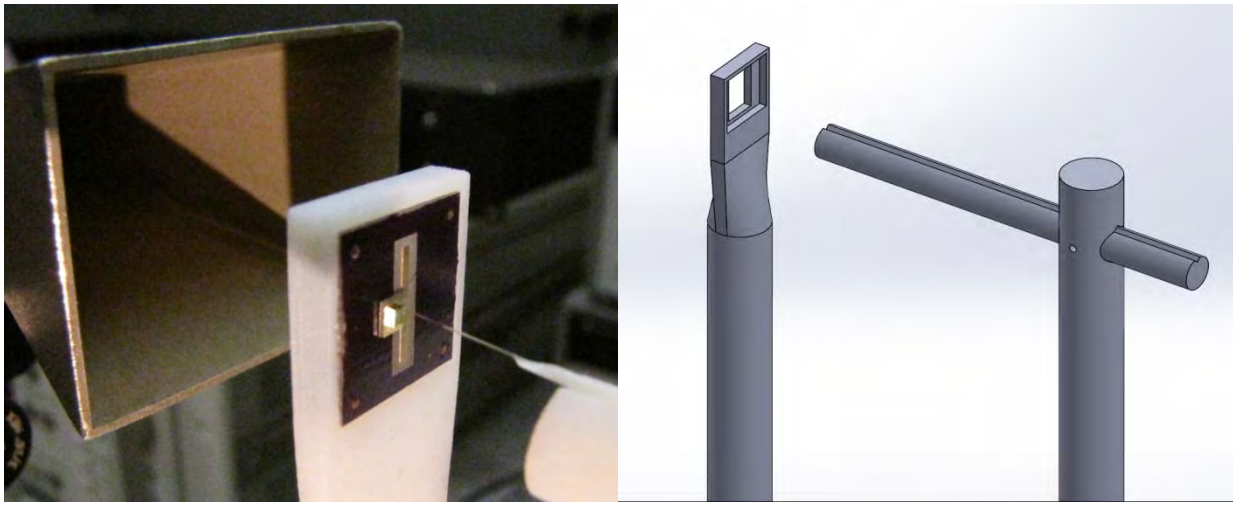

(a) (b)

Fig. 10 – An image of (a) the OMS probe loaded with the MUTC photodiode in front of a Ka-band standard gain horn and (b) a Solidworks model of mounting components for the OMS probe and optical fiber.

6. RESULTS AND FUTURE DEVELOPMENTS

6.1 Pattern Measurements

Figure 11 shows the measured co-polarization, near-field pattern using the PDA and MUTC loaded OMS probes of an open-ended, Ku-band waveguide at 15 GHz. In each case, the probe was 8.5 mm in front of the antenna opening. The probe was raster scanned in a plane of size 128 mm in the H-plane of the antenna and 49 mm in the E-plane of the antenna. The measured near-field pattern using the MUTC loaded probe has some asymmetries in the pattern compared to the PDA loaded probe. The MUTC

photodiode had larger packaging than the PDA photodiode and a metallic backing which caused a geometric asymmetry in the probe. Figure 12 shows the phase contour plots for the near-field amplitude distribution that was shown in Fig. 11.

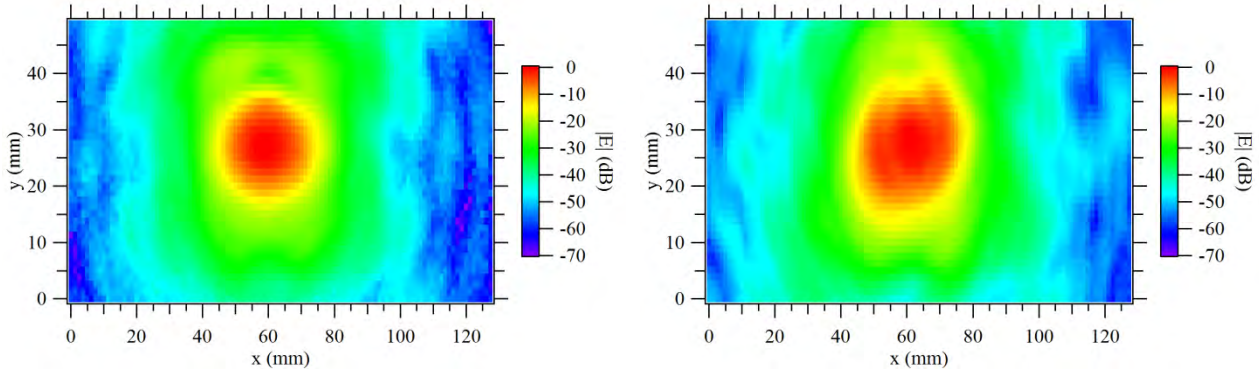

Fig. 11 – The measured near-field pattern of an open-ended Ku-band waveguide at 15 GHz using the PDA (left) and MUTC (right) loaded OMS probe.

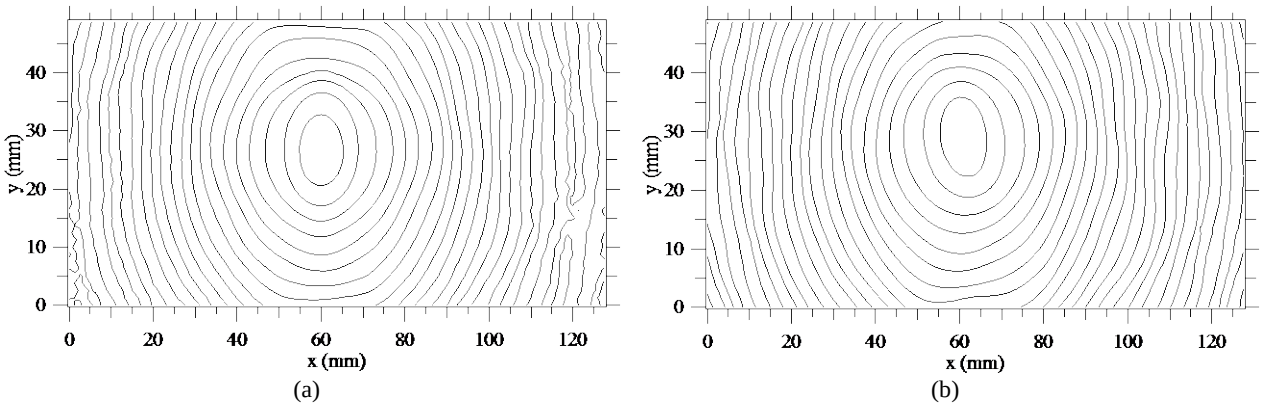

Fig. 12 – The phase contours of a measured near-field pattern of an open-ended Ku-band waveguide at 15 GHz using the PDA (left) and MUTC (right) loaded OMS probe.

6.2 System Linearity

Figure 13 shows a measurement of the linearity for our near-field measurement system using the MUTC-loaded OMS probe. A waveguide variable attenuator was placed behind the AUT that was shown in Figure 1. The placement of this attenuator provides two-way attenuation – the power delivered to the probe is attenuated and the received signal that scattered off of the probe is attenuated. The relative attenuation is normalized such that attenuation below 0 dB begins to compress in the system – a relative attenuation of -5 dB has a compression of 0.8 dB. The solid line in Fig. 13 represents a linear system with a gain of one. The noise floor on the system corresponds to a relative attenuation of 75 dB. Each point between a relative attenuation of 75 dB and -5 dB are within 1.5 dB of an ideal, linear system. For this probe, the system has 80 dB of dynamic range. Due to the monostatic setup, the received amplitude is

proportional to the square of the gain of the antenna – an 80 dB dynamic range corresponds to a dynamic range of 40 dB for an antenna pattern.

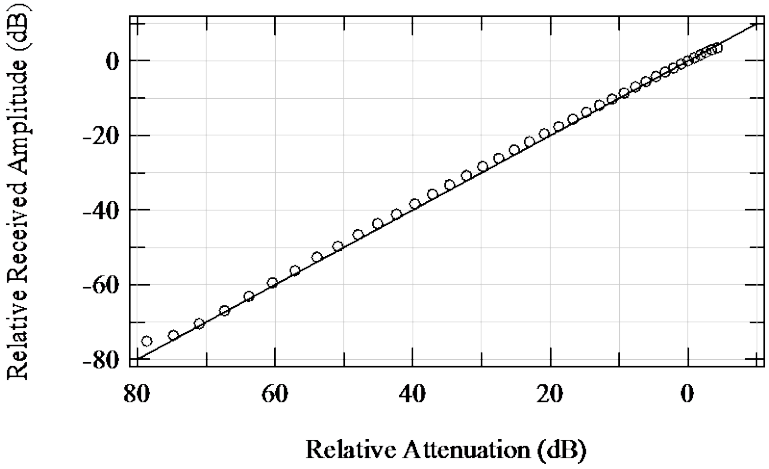

Fig. 13 – A linearity measurement of the OMS near-field measurement system using the MUTC loaded OMS probe.

6.3 Future Developments

In future work, we aim to increase the frequency of our OMS probes into the millimeter-wave region. The photodiodes used here are surface normal devices and are traditionally used for high-power, microwave photonic applications [16]. These devices are less suited for use at frequencies in the millimeter-wave region compared to a uni-traveling carrier (UTC) waveguide structure [19]. In future work we will investigate waveguide photodiodes because they are prime candidates for higher frequency applications due to the decoupling of the transit time (namely the intrinsic region thickness) and device capacitance where the bandwidth is limited by capacitance rather than transmit time [20, 21]. This waveguide style also offers the advantage of integrating the optical coupling into the probe via a photonic integrated circuit [22]. Further developments are ongoing with alternative photodiode structures to make an integrated OMS probe whereas the probe in this report is composed of discrete components that are wire bonded together. The path and length of the wire bonds vary between probes and the elimination of the wire bonds, in favor of an integrated approach, would increase the fidelity of the simulations of the probe RCS.

7. REFERENCES

[1] J. J. Lee, E. M. Ferren, D. P. Woollen, and K. M. Lee, "Near-field probe used as a diagnostic tool to locate defective elements in an array antenna," *Antennas and Propagation, IEEE Transactions on,* vol. 36, pp. 884-889, 1988.

[2] J. Brown and E. V. Jull, "The prediction of aerial radiation patterns from near-field measurements," *Proceedings of the IEE - Part B: Electronic and Communication Engineering,* vol. 108, pp. 635-644, 1961.

[3] A. Neuber, J. Dickens, D. Hemmert, H. Krompholz, L. L. Hatfield, and M. Kristiansen, "Window breakdown caused by high-power microwaves," *Plasma Science, IEEE Transactions on,* vol. 26, pp. 296-303, 1998.

[4] T. E. Tice and J. Richmond, "Probes for Microwave Near-Field Measurements," *Microwave Theory and Techniques, IRE Transactions on,* vol. 3, pp. 32-34, 1955.

[5] A. Henderson, J. R. James, P. Newham, and G. Morris, "Analysis of gating errors in time domain antenna measurements," *Microwaves, Antennas and Propagation, IEE Proceedings H,* vol. 136, pp. 311-320, 1989.

[6] A. G. Yarovoy, T. G. Savelyev, P. J. Aubry, P. E. Lys, and L. P. Ligthart, "UWB Array-Based Sensor for Near-Field Imaging," *Microwave Theory and Techniques, IEEE Transactions on,* vol. 55, pp. 1288-1295, 2007.

[7] J.-C. Bolomey and F. E. Gardiol, *Engineering applications of the modulated scatterer technique*: Artech House, 2001.

[8] A. L. Cullen and J. C. Parr, "A new perturbation method for measuring microwave fields in free space," *Proceedings of the IEE - Part B: Radio and Electronic Engineering,* vol. 102, pp. 836-844, 1955.

[9] J. Richmond, "A Modulated Scattering Technique for Measurement of Field Distributions," *Microwave Theory and Techniques, IRE Transactions on,* vol. 3, pp. 13-15, 1955.

[10] A. M. Vural and D. K. Cheng, "A light-modulated scattering technique for diffraction field measurements," *Radio Sci. J. Res,* vol. 68, pp. 355-362, 1964.

[11] M. A. Abou-Khousa, "Novel modulated antennas and probes for millimeter wave imaging applications," Ph. D. in Electrical Engineering, Electrical and Computer Engineering, Missouri University of Science and Technology, 2009.

[12] M. T. Ghasr, M. A. Abou-Khousa, S. Kharkovsky, R. Zoughi, and D. Pommerenke, "A Novel 24 GHz One-Shot, Rapid and Portable Microwave Imaging System," in *Instrumentation and Measurement Technology Conference Proceedings, 2008. IMTC 2008. IEEE*, 2008, pp. 1798-1802.

[13] H. M. Tehran, J. Laurin, and R. Kashyap, "A low-perturbation near-field imager equipped with optical MST probes," in *Antennas and Propagation, 2009. EuCAP 2009. 3rd European Conference on*, 2009, pp. 3649-3653.

[14] Y. Hu, T. F. Carruthers, C. R. Menyuk, M. N. Hutchinson, V. J. Urick, and K. J. Williams, "Simulation of a partially depleted absorber (PDA) photodetector," *Optics Express,* vol. 23, pp. 20402-20417, 2015.

[15] Z. Li, H. Pan, H. Chen, A. Beling, and J. C. Campbell, "High-Saturation-Current Modified Uni-Traveling-Carrier Photodiode With Cliff Layer," *IEEE Journal of Quantum Electronics,* vol. 46, pp. 626-632, 2010.

[16] M. N. Hutchinson, V. J. Urick, and N. J. Frigo, "Power photodiodes for high dynamic range photonic links," *Applied Optics,* vol. 54, pp. F17-F24, 2015.

[17] V. J. Urick, J. F. Diehl, C. E. Sunderman, J. D. McKinney, and K. J. Williams, "An Optical Technique for Radio Frequency Interference Mitigation," *IEEE Photonics Technology Letters,* vol. 27, pp. 1333-1336, 2015.

[18] U. Gliese, K. Colladay, A. S. Hastings, D. A. Tulchinsky, V. J. Urick, and K. J. Williams, "RF Power Conversion Efficiency of Photodiodes Driven by Mach-Zehnder Modulators," *IEEE Transactions on Microwave Theory and Techniques*, vol. 58, pp. 3359-3371, 2010.

[19] A. Madjar, N. Koka, J. Bloch, M. Draa, and P. M. L. Yu, "A novel analytical model for the UTC-TW photo detector for generation of sub-MM wave signals," in *Microwave Conference, 2007. European*, 2007, pp. 596-598.

[20] M. N. Draa, J. Bloch, D. C. Scott, N. Chen, S. B. Chen, W. S. C. Chang, *et al.*, "Behaviors of the third order intercept point for p-i-n waveguide photodiodes," *Optics Express*, vol. 17, pp. 14389-14394, 2009.

[21] M. N. Draa, D. C. Scott, S. B. Chen, N. Chen, J. Bloch, W. S. Chang, *et al.*, "Voltage-dependent nonlinearities in uni-traveling carrier directional coupled photodiodes," in *Microwave Photonics (MWP), 2010 IEEE Topical Meeting on*, 2010, pp. 15-18.

[22] V. J. Urick, M. J. Mondich, C. E. Sunderman, D. A. Kozak, P. G. Goetz, W. S. Rabinovich, *et al.*, "Microwave Phase Shifting using Coherent Photonic Integrated Circuits," *Journal of Selected Topics in Quantum Electronics*, 2016.